PROCEEDINGS, 48th Workshop on Geothermal Reservoir Engineering
Stanford University, Stanford, California, February 6-8, 2023
SGP-TR-224

Seismic Monitoring of the 2022 Utah FORGE Stimulation: The View from the Surface

Katherine M. Whidden[1], Gesa Petersen[1]*, and Kristine L. Pankow[1]

[1]University of Utah, Salt Lake City, UT

*Current location: GFZ German Research Centre for Geosciences, Potsdam, Germany

Keywords: Utah FORGE, seismicity, seismic monitoring, seismic network, geophones

ABSTRACT

In April 2022, Utah FORGE stimulated the horizontally deviated well 16(A)-32. The stimulation consisted of three stages. The first stimulation was in the open hole and for stages two and three well-casing was perforated. The seismic response from the three stages varied as did the seismic monitoring capabilities from instrumentation in the deep boreholes. Using the seismic data collected in the deep boreholes Geo Energie Suisse (GES) compiled a catalog of 2591 of the best recorded events (M -2.09 to 0.52). In this study, we use data from the local surface and shallow-borehole network and separately from a 208 dense nodal geophone deployment that consisted of 13 patches of 16 nodes each. For the nodal geophone array, we stack the data in each patch and explore how to use the stacked traces for detection, location and source analysis. We explore detection algorithms including energy-based back projection and matched-filters. Detection catalogs are compared to the GES catalog in order to explore how to better incorporate surface seismic instrumentation for monitoring engineered geothermal systems.

1. INTRODUCTION

The Utah Frontier Observatory for Research is Geothermal Energy (FORGE) is a research facility with a mission to enable a commercial pathway for enhanced geothermal energy (EGS). Utah FORGE is located in south central Utah (Figure 1). The crystalline basement reservoir is composed of granitoid and reaches temperatures of ~200°C (Moore et al., 2020). To date the facility includes, the first of two deep (8,500') horizontally deviated wells (16A(78)-32), three deep (> 7,500') boreholes (58-32, 78B-32, and 56-32) available for seismic monitoring, a ~3,500' deep borehole (78-32) instrumented with DAS to depth (note 78B-32 also has usable DAS to ~3,500'), an ~1,000' deep borehole (68-32) instrumented with a three-component geophone and three-component accelerometer (UU.FORK,G[H,N],Z,1,2]), and a local scale seismic network composed of surface and shallow borehole (100 - 150') instrumentation (Figure 1). In the coming year, a second deep deviated well 16B(78)-32 will be drilled. By design 16A(78)-32 is the proposed injection well and 16B(78)-32 the production well.

In April 2022, 16A(78)-32 was stimulated. One of the primary goals of the 2022 stimulation was to map the resulting fracture network with sufficient precision that 16B(78)-32 can be steered to intersect the fractures in order to maximize the probability of connection between the two wells. To achieve the seismic event precision necessary to meet this goal, address seismic hazard concerns, and advance the FORGE mission for a commercial pathway for EGS, three seismic monitoring efforts were undertaken by Utah FORGE. The seismic hazard concerns were addressed using the local scale seismic network (Figure 2a) with magnitude based alarms to trigger based on the Traffic Light System developed for Utah FORGE (Pankow et al., 2020). Utah FORGE partnered with Geo Energie Suisse (GES) for seismic monitoring work of the fracture development within the reservoir. The plan for seismic monitoring included instrumenting the three deep seismic monitoring boreholes (56-32, 58-32, and 78B-32) with geochains at reservoir depth, integrating data from the DAS in 78-32 and 78B-32 and data from a fiber optic BOSS tool, also installed in 78-32 (Rutledge et al., 2021). Unfortunately, the geochains/wirelines failed at the high temperatures encountered at Utah FORGE and the monitoring plan had to be adjusted while in the field. In the end, Stage 1 was monitored with a geochain in 58-32 at maximum depth of 6700'; Stage 2 with the geochain in 58-32 and a two-level analog string in 56-32 at reservoir depth (8315'); and Stage 3 with the same instrumentation from Stage 2 and a geochain in 78B-32 at a maximum depth of 6200'. In addition, in all three stages data from the DAS in 78B-32 and 78-32 and the BOSS tool in 78-32 were integrated into the processing. The varied available geometry of the seismic monitoring between stages led to variation in seismic event resolution with Stage 3 having the highest resolved locations. The GES catalog (https://dx.doi.org/10.15121/1908927) for the 2022 stimulation is the official Utah FORGE catalog for the stimulation.

This paper focuses on the third aspect of seismic monitoring, exploring other, more economically viable, approaches to seismic monitoring. We highlight initial seismic event detection results from the Utah FORGE 2022 stimulation obtained using a dense surface geophone network. This initial detection catalog is compared to the GES event catalog. Advantages of a surface network include reduced costs and easier permitting. Potential short-comings include an inability to telemeter the data for real-time monitoring and reduced sensitivity. This paper provides a baseline for the tradeoffs between surface and borehole networks, in terms of detection thresholds. Future work includes location resolution analysis and incorporating the dense geophone data with the local Utah FORGE network to both improve locations and determine focal mechanisms.

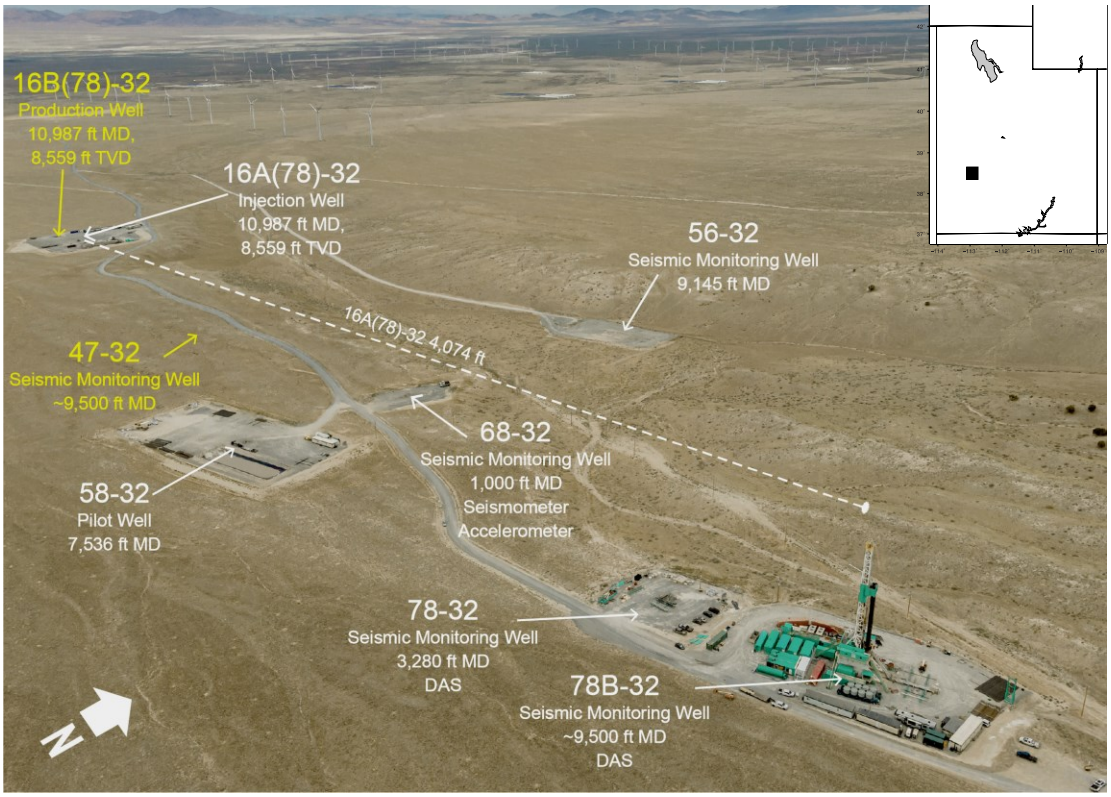

Figure 1. Aerial image of the Utah FORGE site showing locations of several monitoring wells as well as production well 16A-32 (upper left). Dashed line shows the surface projection of well 16A-32 at depth. Yellow font color indicates planned boreholes. Black square in the inset at top right shows the location of Utah FORGE within the state of Utah, corresponding to the map area in Figure 2a.

2. 2022 GEOPHONE ARRAY AND PERMANENT SURFACE NETWORK

Seismic monitoring at Utah FORGE during the April 2022 stimulation consists of a permanent local network of surface and borehole instruments, and a temporary geophone array that was in place from April 4-May 5 (Figure 2). The local network is configured in two concentric rings centered on the stimulation area with radii of 3 and 8 km, with a few outlying stations. Of the ten surface stations, seven are broadbands (FOR[1,2,5,6,7,8,U],), two are accelerometers (FORB, MHS2), and one is a short period instrument (NMU). Seven stations are shallow boreholes; three are co-located broadband and accelerometer instruments at 30 m depth (FSB[1,2,3]), three are broadbands at 40 m depth (FSB[4,5,6]), and one is a short period and accelerometer at 305 m depth (FORK).

The temporary geophone array consists of 207 three component Fairfield ZLand geophones organized in groups of 16, with a 4 x 4 geometry and a spacing of 30 m, with an aim to stack signals from each patch and increase the signal to noise ratio. The locations of the groups were selected to be optimally oriented around the stimulation at the toe of well 16A(78)-32, and close enough to roads to minimize overland carrying of heavy instruments. A team of six UUSS employees, post-docs, and graduate students deployed the geophone stations in the field. The original plan was to measure the 30 m spacing between stations precisely with a measuring tape. Upon arrival, the high winds for which the FORGE area is famous made that plan impossible. Instead, station locations were determined with handheld GPS units. In hindsight, topography and vegetation would have made the tape measurements difficult and less accurate over a distance of 30 m, and GPS was a better choice. Another challenge was carrying the nodes to more remote areas. Each node weighs ~6 lbs (~2.7 kg) and several were carried in large backpacks. The deployment schedule maximized the most available team members for the furthest walks. Each node was installed flush with the ground surface after digging a shallow hole with a shovel (Figure 3). This level of burial allowed for minimal wind noise while also allowing the retrieval team to find the instruments easily. During retrieval, the Utah Geological Survey performed a high-precision GPS survey of the nodal locations.

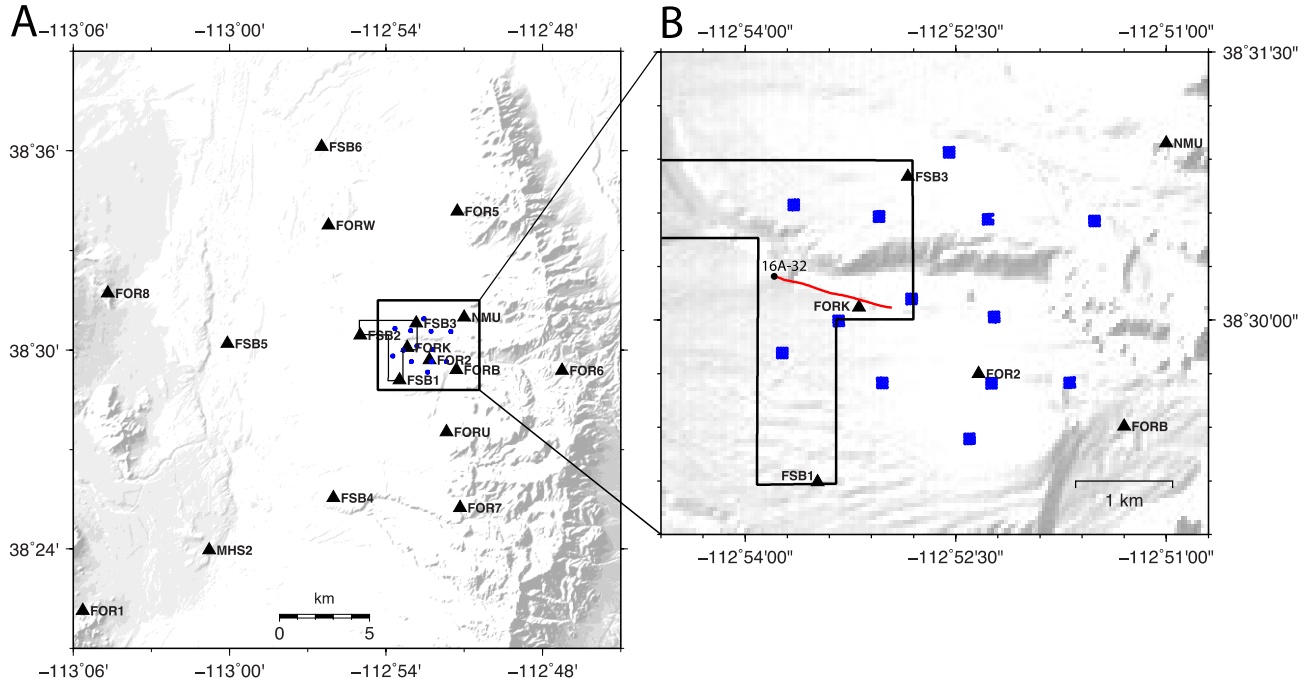

Figure 2. (A) Maps of the permanent seismic network (black triangles) and (B) temporary nodal deployment (blue squares). Each blue square represents sixteen nodal stations in a 4 x 4 grid. Black circle is the 16A-32 wellhead and the red line is the surface projection of the well at depth.

Figure 3. A UUSS student installs a nodal station at the Utah FORGE site. Instrument is placed in a shallow hole so that the top is flush with the ground surface.

3. METHODS

3.1 Waveform Stacking

We stack the continuous waveforms of each patch of 4x4 geophones to improve the signal to noise ratio for event detections. We apply time shifts to account for the event-station distances of the 16 stations of each patch. The time shifts were computed using a local 1D velocity model and the location of the largest earthquake from the GES catalog. Resulting time shifts are on the order of 0.003-0.02 s, corresponding to up to 12 samples at a sampling rate of 500 Hz. The stacking clearly improves the signal to noise ratio, suppressing noise and emphasizing P and S arrivals as well as a P-S converted phases (e.g. Figure 4).

Waveform spectra of vertical component stacks of all station patches show that noise levels are high up to 15 or 20 Hz. P-phase arrivals are clearly seen at frequencies of about 20-60 Hz with signals being visible up to 100 Hz (Figure 5). The single patches show significant differences in their SNR levels, reflecting not only station-event distances, but also local noise conditions due to operations at the borehole platforms, moving vehicles and wind conditions. Based on the spectral observations, we choose a frequency band of 20-50 Hz for detecting events.

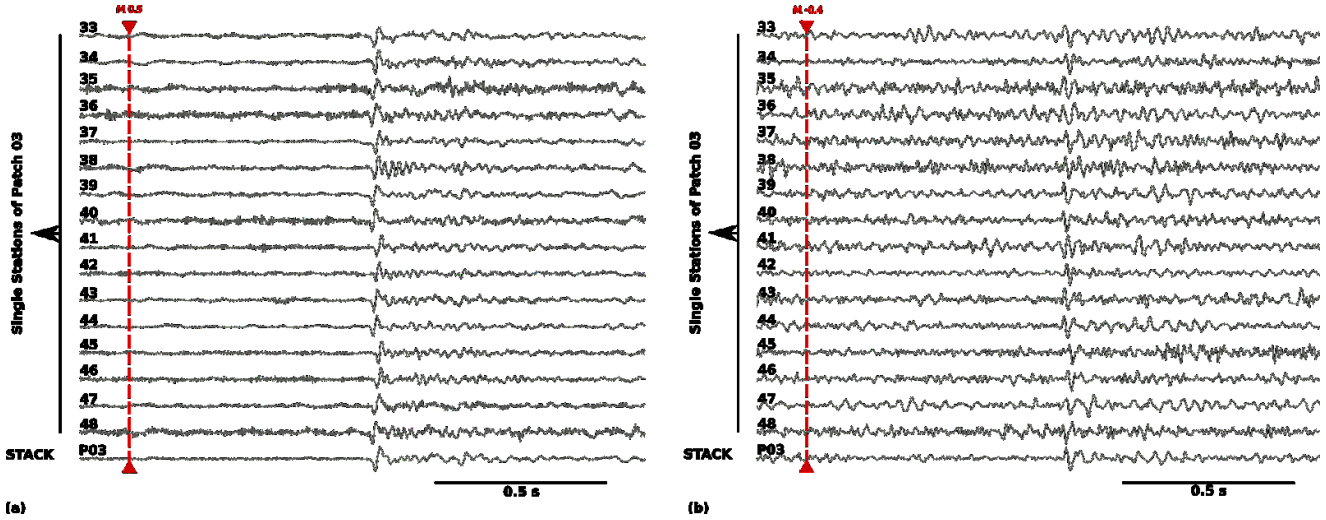

Figure 4: Waveform examples patch 3, stations 33-48 and stack. Vertical component. (a) shows the largest event (M 0.5; not filtered) and (b) a M -0.4 event (BP filter 20-80 Hz), both during injection stage 3.

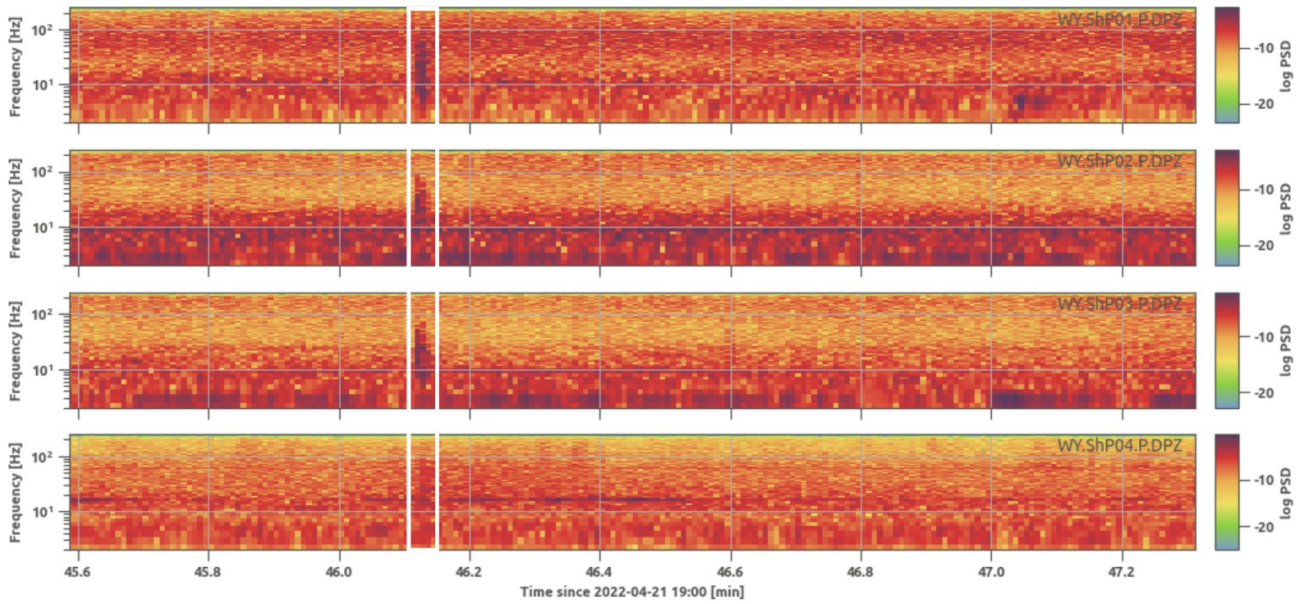

Figure 5: Spectrograms of stacked vertical waveforms, patches 1 (top) to 4 (bottom). The white box marks the location of the largest event of stage 3 (M 0.5).

3.2 Event Detection

We applied the waveform coherency-based detection and location tool *Lassie* (https://git.pyrocko.org/pyrocko/lassie) of the pyrocko ecosystem (Heimann et al., 2017) to detect induced events during the first eight hours of stage 3 of the 2022 stimulation. *Lassie* computes theoretical receiver arrival times for each point on a 3-D spatial grid (3x3x3 km around the injection, step size 100m) using a 1-D velocity model in moving time windows. Characteristic functions (CF) are computed for each time window according to the theoretical arrival time grid. If the CF exceeds a defined threshold, a detection is declared with an origin time and preliminary location on the grid. In this study, we compute the CF based on STA/LTA to detect impulsive P-phase arrivals (short window 0.05 s, long window 1s) and energy wave packet image functions that are sensitive to energetic S phases which may have emergent onsets. Based on the spectras presented above, we apply a bandpass filter between 20 and 50 Hz. Note that the step size of the spatial grid is too coarse for any structural interpretation of the detection-event-locations. The settings of the characteristic function were optimized to reliably detect events from the source area surrounding the borehole, not to locate them. For more exact locations, the frequency band chosen in this step is not sufficient.

4. RESULTS

Figure 6 shows waveform examples of three seismic events that were detected during stage 3. Events with magnitudes around 0 are reliably seen on most stacks, while events with magnitudes around M -0.4 are still visible on at least half of the patches. The third example for a M -0.7 shows that detections of such low magnitudes are still possible. In comparison to the GES catalog for the same 8-hour time period, we detect 90% of the GES events with $M \geq -0.4$, 87% with $M \geq -0.5$ and 76 % with $M \geq -0.6$. For events with CF values corresponding to events with M -0.7 and below, we find many false detections. Therefore, we plan to add a second processing step based on a spectral classification to distinguish true and false detections that have lower CF values.

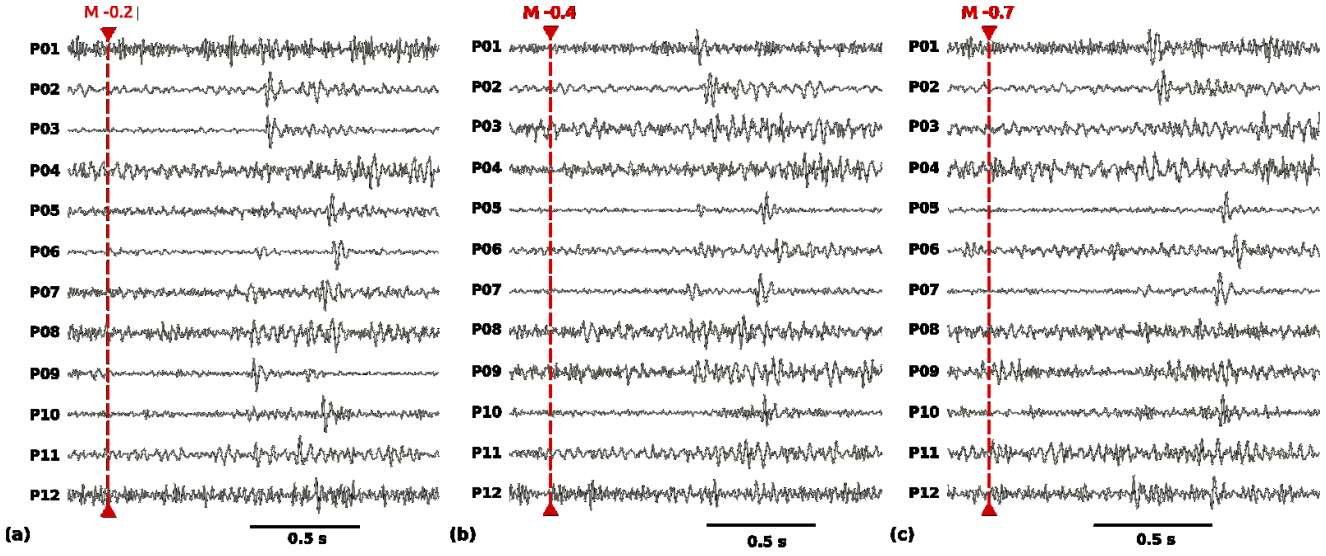

Figure 6: Examples of detected events with magnitudes M -0.2 (a), M -0.4 (b) and M -0.7 (c), magnitudes are from GES catalog. Shown are stacked waveforms of the vertical components, BP filter 20-80 Hz.

5. DISCUSSION

Thus far, we have determined that we can use the described network geometry and detection algorithm to reliably detect small earthquakes down to at least M -0.7. However questions about our ability to locate these earthquakes with sufficient precision still remain. Ultimately we would like to determine whether a surface network is capable of replacing expensive borehole monitoring to determine fracture growth patterns and locations. This question will be answered in future location studies using this dataset.

Mesimeri et al. (2021b) conducted a similar experiment of detecting microseismicity at Utah FORGE in April 2019 using a surface geophone network. The Mesimeri et al. (2021b) study varies from this study in that the geophone network was composed of 151 stations organized into a circular array with a maximum aperture of ~5 km, consisting of five concentric rings with radii ranging from 100 m to 2500 m centered on the test injector well 58-32. In addition, they employed a frequency-domain detector and used backprojection to determine locations for the detections. The 2019 stimulation was much smaller than the 2022 stimulation (Moore et al., 2020) and the largest earthquake measured was an M -0.5 (Bradshaw et al., 2022). The frequency domain detector was applied to two hours of data during the 2019 stimulation. The earthquake catalog compiled by Schlumberger in 2019 contains 61 seismic events ($-1.9 \leq M \leq -0.5$) and the frequency domain detector identified six events ($-1.8 \leq M \leq -0.5$). It is difficult to directly compare the results from the station geometries and detection algorithms of Mesimeri et al. (2021b) and those of this study due to the difference in injection volume and

earthquake magnitudes between the two experiments. However, a couple of key observations can be made: (1) the Mesimeri et al. (2021b) station geometry and frequency-domain detector had a lower detection threshold (M -1.8) and can detect earthquakes with little visible signal in the time domain, however, < 10% of the available events were detected and phase information that is used in traditional seismic event location algorithms may not be identified; and (2) the network geometry and detection algorithm in this study identifies a more uniform catalog, although with a higher detection threshold, and since the events are detected at multiple patches the data can be integrated into location algorithms.

This and the Mesimeri et al. (2021b) studies show the promise of using surface geophones for geothermal reservoir monitoring. There will be tradeoffs in detection thresholds and location resolution, more detailed exploration of these tradeoffs is part of on-going work. Additionally, future work with this dataset includes catalog location, relative relocation, and further catalog enhancement with a matched-filter technique similar to Mesimeri et al. (2021a) and Whidden et al. (2023). We also will explore first motion focal mechanisms by stacking signals from each patch as described above to enhance the signal-to-noise ratio of the first motions.

6. CONCLUSIONS

We have presented here detection results using a network geometry that allows for improved signal-to-noise ratio by stacking recordings from 16 closely located stations, allowing for reliable detection of earthquakes down to M -0.7. This study is part of an ongoing effort to examine different surface network geometries and detection algorithms to maximize catalog enhancement at Utah FORGE. This study is still a work in progress and future work includes earthquake locations, continued catalog enhancement through a matched-filter method, and first motion focal mechanisms.

ACKNOWLEDGMENTS

Thank you to Patrick Bradshaw, Zachary Claerhout, Daniel Wells, and J. Mark Hale for help deploying and collecting nodal instruments in the field, and to Ben Erickson and the Utah Geological Survey for the high-resolution GPS survey of the nodal network. Funding was provided by DOE EERE Geothermal Technologies Office under Project DE-EE0007080 Enhanced Geothermal System Concept Testing and Development at the Milford City, Utah Frontier Observatory for Research in Geothermal Energy (FORGE) site and the State of Utah. The support and resources from the Center for High Performance Computing at the University of Utah are gratefully acknowledged.

REFERENCES

Bradshaw, P., G. Petersen, and K. Pankow (2022). Characterizing the induced microseismicity of the 2019 Utah FORGE well stimulation, GRC transactions, 46, Reno, Nevada.

Heimann, Sebastian; Kriegerowski, Marius; Isken, Marius; Cesca, Simone; Daout, Simon; Grigoli, Francesco; Juretzek, Carina; Megies, Tobias; Nooshiri, Nima; Steinberg, Andreas; Sudhaus, Henriette; Vasyura-Bathke, Hannes; Willey, Timothy; Dahm, Torsten (2017): Pyrocko - An open-source seismology toolbox and library. V. 0.3. GFZ Data Services. https://doi.org/10.5880/GFZ.2.1.2017.001

Mesimeri, M., Pankow, K.L., Baker, B., and Hale, J.M. (2021a). Episodic earthquake swarms in the Mineral Mountains, Utah driven by the Roosevelt hydrothermal system, J. Geophys. Res.: Solid Earth, 126, e2021JB021659. https://doi.org/10.1029/2021JB021659.

Mesimeri, M., Pankow, K.L., and Rutledge, J. (2021b). A Frequency-Domain-Based Algorithm for Detecting Microseismicity Using Dense Surface Seismic Arrays. Bull. Seism. Soc. Am. 111 (5): 2814–2824. doi: https://doi.org/10.1785/0120210062

Moore, J., McLennan, J., Pankow, K.L., Podgorney, R., Simmons, S., Wannamaker, P., Jones, C., Rickard, W., Barker, B., Hardewick, C., and Kirby, S. (2020). Overview of Utah FORGE results in 2019: Proceedings, 45th Workshop on Geothermal Reservoir Engineering, Stanford University, CA February 10- 12, 10 p.

Pankow, K., Rutledge, J., & Wannamaker, P. (2020). Utah FORGE Induced Seismicity Mitigation Plan . United States. https://gdr.openei.org/submissions/1319

Rutledge, J, K. Pankow, B. Dyer, P. Wannamaker, P. Meier, F. Bethmann, and J. Moore (2021). Seismic monitoring at the Utah FORGE EGS Site, GRC Transactions, 45, 12 pp.

Whidden, K.M., Petersen, G., Mesimeri, M., and Pankow, K.L. (2023) Analysis of the 2021 Milford, Utah earthquake swarm: Enhanced earthquake catalog and migration patterns, Front. Earth Sci. 11, accepted. doi: 10.3389/feart.2023.1057982